A Wireless, Passive Carbon Nanotube-Based Gas Sensor

Keat Ghee Ong, Kefeng Zeng, and Craig A. Grimes, *Member, IEEE*

***Abstract*—A gas sensor, comprised of a gas-responsive multiwall carbon nanotube (MWNT)—silicon dioxide (SiO_2) composite layer deposited on a planar inductor-capacitor resonant circuit is presented here for the monitoring of carbon dioxide (CO_2), oxygen (O_2), and ammonia (NH_3). The absorption of different gases in the MWNT-SiO_2 layer changes the permittivity and conductivity of the material and consequently alters the resonant frequency of the sensor. By tracking the frequency spectrum of the sensor with a loop antenna, humidity, temperature, as well as CO_2, O_2 and NH_3 concentrations can be determined, enabling applications such as remotely monitoring conditions inside opaque, sealed containers. Experimental results show the sensor response to CO_2 and O_2 is both linear and reversible. Both irreversible and reversible responses are observed in response to NH_3, indicating both physisorption and chemisorption of NH_3 by the carbon nanotubes. A sensor array, comprised of an uncoated, SiO_2 coated, and MWNT-SiO_2 coated sensor, enables CO_2 measurement to be automatically calibrated for operation in a variable humidity and temperature environment.**

***Index Terms*—Ammonia, carbon dioxide, carbon nanotube, gas sensor, oxygen, remote query.**

I. Introduction

CARBON nanotubes have found application as field emission devices [1], electronic switches [2]–[5], actuators [6], and random access memory [7]. Recently, application of carbon nanotubes as oxygen [8] and methane [9] gas sensors has been reported; since nanotubes are essentially all surface, they offer the possibility of excellent sensitivity and rapid response times.

Gas sensors are used in many industrial, medical, and commercial applications. For example, oxygen sensors are used in the monitoring of combustion engine environment to increase engine performance and reduce emission of green house gases [10]. Ammonia sensors are important for monitoring ambient ammonia concentration since it is related to many environmental issues such as acidification, human health, and climate change through particle formation [11]. In addition to controlling industrial processes [12] and monitoring air quality [13], CO_2 sensors are also widely used in food and medicine packages as a means of detecting spoilage [14], [15]. Most gas sensors available on the market today operate by measuring the impedance of a capacitor coated with a gas-responsive polymer(s) or ceramic such as heteropolysiloxane [16], $BaTiO_3$ [17], CeO/$BaCO_3$/CuO [18], Ag_2SO_4 [19], Na_2CO_3 [19], SnO_2, etc. These gas sensors offer a high degree of accuracy and reliable performance, but require hard-wire connections between the sensor head, power supply, and data processing electronics which precludes many monitoring applications.

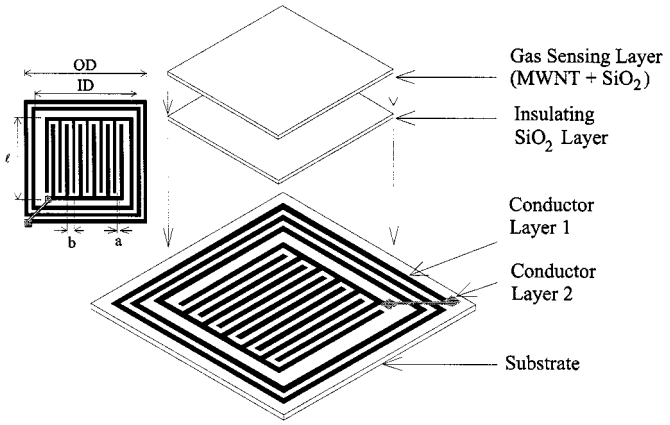

Fig. 1. Schematic drawing of the MWNT gas sensor. A planar inductor-interdigital capacitor pair is photolithographically defined upon a copper clad printed circuit board. The capacitor is first coated with a protective electrically insulating SiO_2 layer followed by a layer of gas responsive MWNT-SiO_2 composite.

In this paper, we report the application of multiwall carbon nanotubes (MWNTs) for remote query detection of carbon dioxide, oxygen, and ammonia based upon the measured changes in MWNT permittivity and conductivity with gas exposure. The transduction platform used in this work is a planar, inductor-capacitor resonant-circuit (LC) sensor [20], [21]. A thin layer of gas-sensitive MWNT-SiO_2 composite is placed upon the interdigital capacitor of the LC sensor; as the permittivity and/or conductivity of the adjacent MWNT-SiO_2 composite changes, so does the sensor resonant frequency that remotely monitored through a loop antenna [20]. The passive nature of the LC sensor enables long term monitoring without battery lifetime issues, and the wireless nature of the platform enables long-term gas monitoring from within sealed, opaque containers.

II. Sensor Design and Operation

The general sensor structure is shown in Fig. 1. It consists of a printed inductor-capacitor resonant circuit that is first coated with a protective, electrically insulating SiO_2 layer [22] (see Fig. 2), followed by a second layer of gas-responsive MWNT-SiO_2 mixture with the SiO_2 matrix acting to physically bind the MWNTs to the sensor. As the sensor is exposed to various gases, the relative permittivity ε_r' and the conductivity (proportional to ε_r'' [23]) of the MWNTs vary, changing the

Manuscript received April 18, 2001; revised February 1, 2002. This work was supported by the National Science Foundation under Grants DMR-9 809 686 and ECS-9 875 104.The associate editor coordinating the review of this letter and approving it for publication was Dr. Vladimir Lumelsky.

The authors are with the Department of Electrical Engineering & Materials Research Institute, Pennsylvania State University, University Park, PA 16802 USA (e-mail: cgrimes@engr.psu.edu).

Publisher Item Identifier S 1530-437X(02)03942-8.

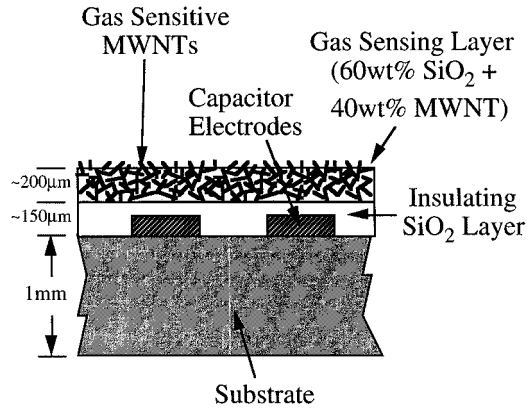

Fig. 2. Cross-sectional view of the interdigital capacitor. An electrically insulating 150 μm-thick SiO_2 layer is first applied to protect the sensor, followed by a 200 μm MWNT-SiO_2 gas-sensing layer.

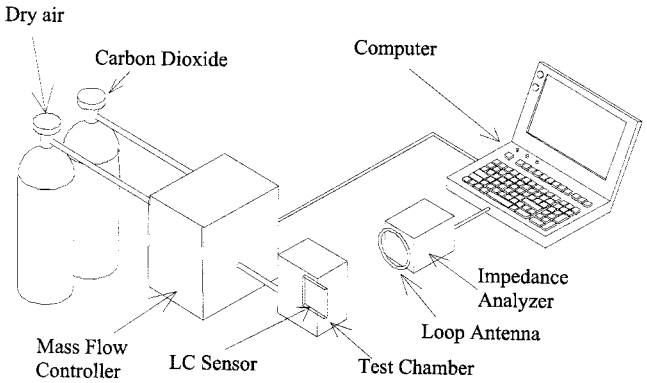

Fig. 3. Experimental setup for testing the gas sensor. The sensor is placed inside a sealed Plexiglas chamber and monitored via a loop antenna. An impedance analyzer is used to measure the impedance spectrum across the terminals of the antenna, and a mass-flow controller is used to control the flow rates of different gasses. A computer controls the devices via the GPIB interface.

effective complex permittivity of the coating and hence the resonant frequency of the sensor. The relationship between CO_2, O_2, and NH_3 adsorption and the complex permittivity is discussed within Section IV.

The frequency spectrum of the sensor is obtained by directly measuring the impedance spectrum of a sensor-monitoring loop antenna (see Fig. 3). The impedance of the loop antenna is removed from the measurement using a background subtraction, obtained by measuring the antenna impedance without the sensor present. A typical background-subtracted impedance spectrum is shown in Fig. 4, where the resonant frequency f_0 is defined as the frequency at the maximum of the real impedance (resistance), and the zero-reactance frequency f_Z is the frequency where the imaginary impedance (reactance) goes to zero. By modeling the sensor with an RLC circuit and performing standard circuit analysis, the complex permittivity, $\varepsilon_r' - j\varepsilon_r''$, of the coating material (both the MWNT-SiO_2 and SiO_2 layers together) is calculated from the measured f_0 and f_Z values [20], [21]

$$\varepsilon_r' = \frac{1}{(2\pi f_0)^2 L\kappa\varepsilon_0} - \varepsilon_S$$
$$\varepsilon_r'' = \frac{\sqrt{f_0^2 - f_Z^2}}{4\pi^2 f_0^3 L\kappa\varepsilon_0} \tag{1}$$

where ε_0 is the free space permittivity ($\varepsilon_0 = 8.854 \times 10^{-12}$F/m), ε_s is the relative permittivity of the electrically

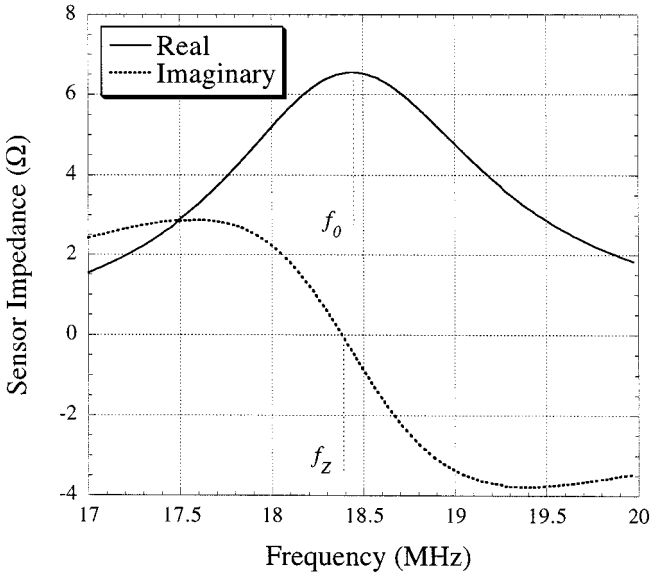

Fig. 4. An illustrative measured impedance spectrum of the sensor-perturbed antenna, after subtracting the background antenna impedance. The resonant frequency f_0 is defined as the maximum of the real portion of the impedance, and the zero-reactance frequency f_Z is the zero crossing of the imaginary portion of the impedance spectrum.

lossless substrate (that is $\varepsilon_s = \varepsilon_s'$), κ is the cell constant of the interdigital capacitor, and L is the inductance of the spiral inductor in Henry's. The cell constant κ and inductance L can be calculated from the sensor geometry using [24]–[26]

$$\kappa = \frac{\ell(N_C - 1)K[(1-(a/b)^2)^{1/2}]}{2K[a/b]} \tag{2}$$
$$L = 1.39 \times 10^{-6}(\mathrm{OD} + \mathrm{ID})N_L^{5/3}\log_{10}\left(4\frac{\mathrm{OD}+\mathrm{ID}}{\mathrm{OD}-\mathrm{ID}}\right) \tag{3}$$

where a, b, ℓ, OD, and ID are the dimensions of the sensor defined in Fig. 1, N_C is the number of fingers in each capacitor's electrode, N_L is the number of inductor turns, and K is the elliptic integral of the first kind.

III. Experimental

A. Preparation of Carbon Nanotubes

The MWNTs used in this work were prepared by pyrolysis of ferrocene and xylene under Ar/H_2 atmosphere over quartz substrates in a two-stage reactor [27]. Approximately 6.5 mol% of ferrocene, which functions as a precursor for producing Fe catalyst particles, was dissolved in xylene hydrocarbon fuel and continuously fed into a tubular quartz reactor. The liquid feed was passed through a capillary tube and preheated to ≈175 °C prior to its entry into the furnace. At this temperature, the liquid exiting the capillary was immediately volatilized and swept into the reaction zone of the furnace by a flow of argon with 10% hydrogen. The MWNTs grow perpendicularly from the surface of the quartz reactor tube. After the reaction, the pre-heater and the furnace were allowed to cool to room temperature in flowing argon, and the MWNT sheets were collected.

The resulting MWNTs were characterized by field-emission scanning electron microscopy. These studies confirm the

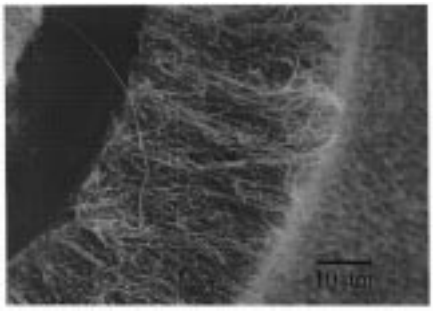

Fig. 5. Field-emission scanning electron microscope image of the as-fabricated MWNTs. The MWNT mat consists of highly aligned MWNTs with the dominant tube diameter in the range 20–25 nm with length 50 μm.

collected material consists of highly aligned MWNTs with the dominant tube diameter in the range 20–25 nm with length $\approx 50\,\mu$m. Fig. 5 is a field-emission scanning electron micrograph image of some resulting MWNTs. The MWNT clumps were placed in toluene and then sonicated for 30 min to disperse the individual nanotubes, rinsed with isopropanol alcohol, and then allowed to dry. The nanotubes were then dispersed in a liquid SiO_2 solution (20 wt% SiO_2 nanoparticles dispersed in water, from [22]) such that a nanotube to SiO_2 dry-weight balance of 2:3 was obtained. The resulting solution was pipetted onto the interdigital capacitor of the sensor and dried in room temperature.

B. Sensor Fabrication

A 2-cm square sensor was fabricated by photolithographically patterning a square spiral inductor and an interdigital capacitor on a printed circuit board (PCB) (see Fig. 1). A $\approx 150\,\mu$m thick layer of SiO_2 (confirmed by SEM imaging) followed by an $\approx 200\,\mu$m thick layer of MWNT-SiO_2 mixture were then coated onto the capacitor of the sensor, with a resulting sensor cross section as shown schematically in Fig. 2.

C. Experimental Setup

The testing facility is schematically depicted in Fig. 3. The sensor was placed inside a sealed Plexiglas test chamber, and monitored with a single-turn 16 cm diameter loop-antenna located approximately 15 cm from the sensor. Test gas concentration was controlled with a mass flow controller (MKS Instruments multi gas controller 647B). The antenna impedance was measured with an impedance analyzer (Hewlett Packard 4396B), with the cable length removed from the measurement using an HP85033D calibration kit. A computer was used to control the mass flow controller and the impedance analyzer via GPIB interface, as well as analyzing and processing the measurements.

IV. Results & Discussion

A. CO_2 Detection

Fig. 6 shows the response of the sensor as it is alternately cycled between dry air ($\sim$80% N_2 and 20% O_2) and pure CO_2 at 0% RH and 23 °C. There is a decrease in values of ε_r' and ε_r'', approximately $-0.040(-0.91\%)$ and $-0.035(-4.40\%)$, respectively, as the gas is switched from dry air to CO_2. The change in the complex permittivity magnitude $|\varepsilon_r|$ is -1.02%. The change in the complex permittivity is reversible, with no hysteresis observed.

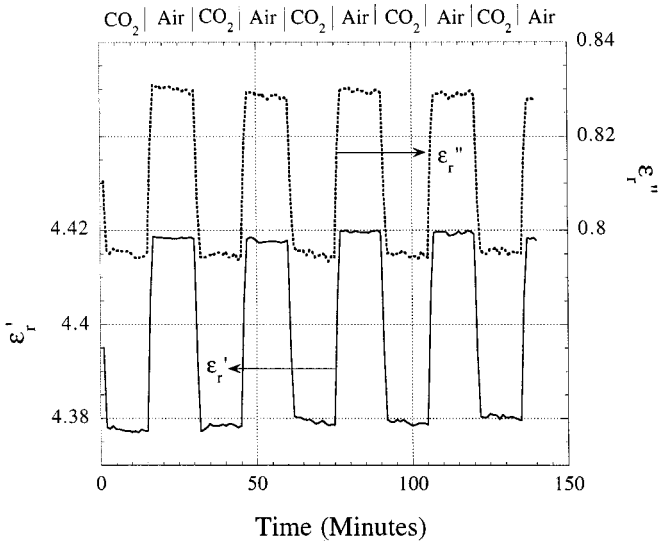

Fig. 6. Measured ε_r' and ε_r'' values when the sensor is cycled between pure CO_2 and dry air. The changes are reversible, without hysteresis between increasing and decreasing CO_2 concentrations.

As seen in Fig. 6 both ε_r' and ε_r'' of the MWNTs are lower when the sensor is exposed to CO_2 and higher when the sensor is exposed to dry air containing $\sim$80%N_2 and 20% O_2. We believe that the change in ε_r'', which is directly proportional to the conductivity $\sigma = 2\pi f \varepsilon_0 \varepsilon_r''$, is due to the adsorption and/or the insertion of CO_2 molecules into either the core or surface of the MWNT. Earlier work has shown that some of the MWNTs behave as p-type semiconductors [28]; for these MWNTs the adsorbed CO_2, which is a reducing agent, injects electrons into MWNTs and decreases the conductivity and ε_r''. In addition, CO_2, with two lone pair of electrons in a Π-type $C = 0$ binding [29], has a higher absorption capacity compared to N_2, which is an inert diatomic molecule that only reacts to graphene at high temperature [30]. The absorption of more CO_2 molecules into the MWNT layer decreases the effective ε_r' of the MWNT layer since N_2 and CO_2 have a much lower $\varepsilon_r'(\approx 1)$ compared to the MWNT graphene layer $(\varepsilon_r' \approx 15)$.

Fig. 7 presents ε_r' and ε_r'' as a function of the CO_2 to dry air volume ratio. The symmetry of the steps indicates the absence of hysteresis with increasing or decreasing CO_2 concentrations. The absolute change in the complex permittivity with CO_2 concentration is linear at $\Delta\varepsilon_r' = -0.000\,404\,3/\%CO_2$ and $\Delta\varepsilon_r'' = -0.000\,347\,6/\%CO_2$.

B. O_2 Detection

Fig. 8 shows the response of the sensor as it is alternately cycled between N_2 and O_2; the humidity level in the chamber was 0% RH, and the temperature was 23 °C. There is a decrease in ε_r' of $-0.004(-0.09\%)$ and an increase in ε_r'' of 0.0025 (0.31%) as the gas is switched from N_2 to O_2. The change in the complex permittivity magnitude $|\varepsilon_r|$ is -0.07% with no hysteresis observed. The changes in both ε_r' and ε_r'' in response to O_2 are about ten times smaller compared to that of CO_2.

The increase in ε_r'' (conductivity) at high O_2 concentrations is due to the oxidizing capability of O_2; as O_2 is absorbed in the MWNT layer, it extracts electrons from the p-type MWNTs [28], increasing the number of holes in the material and consequently

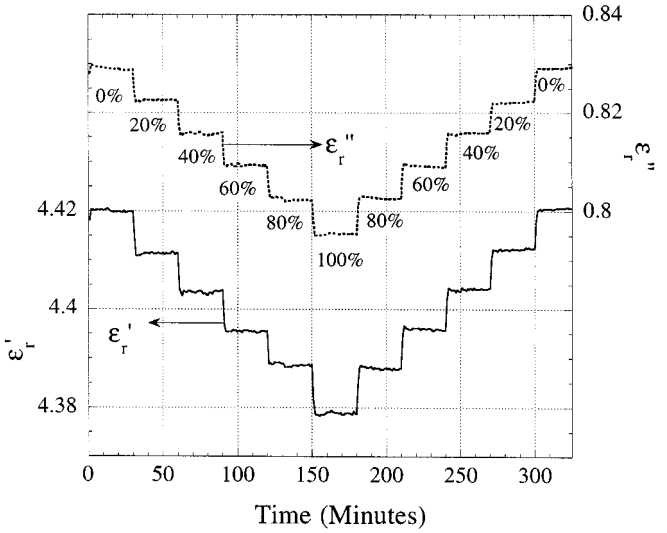

Fig. 7. Measured ε_r' and ε_r'' values when the sensor is exposed to CO_2 concentrations varying from 0% (volume) to 100% and then back to 0%. The shifts are linear, with $\Delta\varepsilon_r' = -0.000\,404\,3/\%CO_2$ and $\Delta\varepsilon_r'' = -0.000\,347\,6/\%CO_2$.

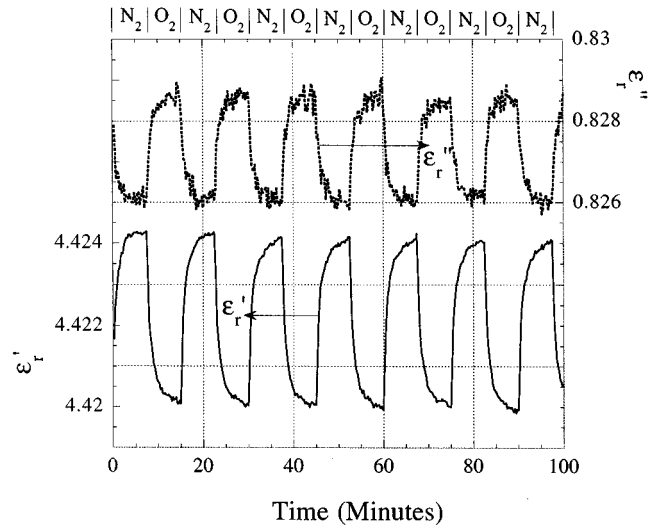

Fig. 8. Measured ε_r' and ε_r'' values when the sensor is cycled between pure O_2 and N_2. The changes are reversible, without hysteresis between increasing and decreasing O_2 concentrations.

increasing ε_r''. Since O_2 has a higher absorption capacity compared to N_2, the effective ε_r' of the MWNTs decreases with increasing O_2 concentration because more O_2 molecules are absorbed in the MWNTs. The smaller change in both ε_r' and ε_r'' compared to CO_2 indicates MWNTs have a lower affinity for O_2.

C. NH_3 Detection

The response of the sensor when it was cycled between NH_3 and N_2 is shown in Fig. 9. As can be seen from the plot, the sensor shows a reversible change in ε_r' and ε_r'', about 0.09 (2%) and $-0.06(-7.5\%)$, respectively, when switching from N_2 to NH_3, as well as an irreversible increase in ε_r' and decrease in ε_r'' throughout the duration of the experiment. The measured changes in the complex permittivity are approximately twice that seen in response to CO_2, indicating the MWNTs have a higher affinity for NH_3.

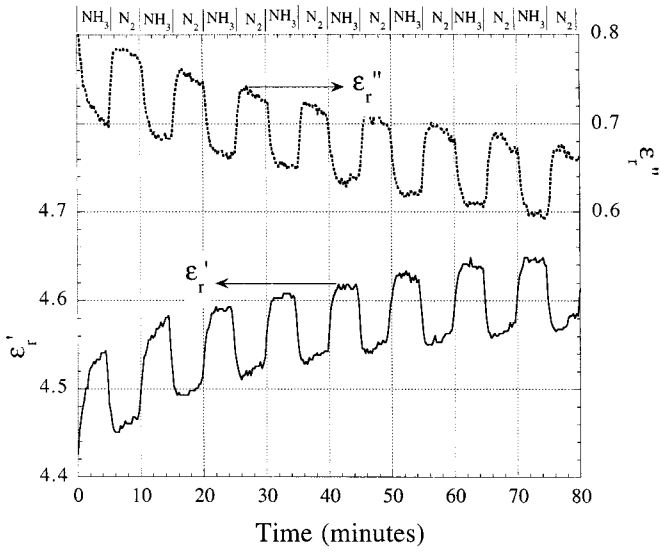

Fig. 9. Measured ε_r' and ε_r'' values when the sensor is cycled between NH_3 and N_2. The changes are irreversible due to the chemisorption of NH_3 to the MWNTs that cannot be simply removed by passing N_2.

In general, ε_r' of the MWNT layer is higher when the sensor is exposed to NH_3 because ε_r' of NH_3 is 19, much larger than N_2, which is ≈ 1. Since NH_3 is a reducing agent, the absorption of NH_3 molecules will inject electrons to the MWNTs and decrease the number of conducting holes in the p-type MWNTs, decreasing the conductivity and ε_r''.

The reversible and irreversible responses of the sensor to NH_3 are caused by the difference in the NH_3-MWNT bonding mechanisms. Ammonia molecules are absorbed into MWNTs through two mechanisms: physisorption (a weak bond) and chemisorption (a strong bond). When switching from NH_3 to N_2, the weak electrostatic bonds between the physisorbed NH_3 and MWNTs are overcome by the kinetic energy of the moving N_2 molecules, which results in the release of the physisorbed NH_3 and causes a reversible change in the complex permittivity. Conversely, the bonds between the chemisorbed NH_3 molecules and MWNTs are very strong and cannot be broken by simply passing N_2 gas. Hence, as the sensor goes through NH_3-N_2 cycles there is a buildup in chemisorbed NH_3 on the MWNT surface, which causes an irreversible change in the complex permittivity. Due to the existence of both irreversible and reversible responses, depending upon the time exposure of the sensor, the MWNTs can be used as a sensor and/or a dosimeter. The MWNT-dosimeter/sensor can detect a quick variation, in the range of a few minutes, in NH_3 concentrations, as well as monitor the slow buildup of NH_3 in the duration of a few hours or days.

D. Sensor Response Time

The response time of the sensor t_R is defined as the time to achieve a steady state response after switching gas concentrations. The response time for CO_2 detection is determined from Fig. 10 as approximately 45 s, and was found to be constant with temperature to 43 °C, the upper limit tested. Operation at elevated temperatures improves the response time of the sensor as it is cycled between dry and humid environments. Switching from 0% to 100% humidity levels at 23 °C, 31 °C, and 42 °C

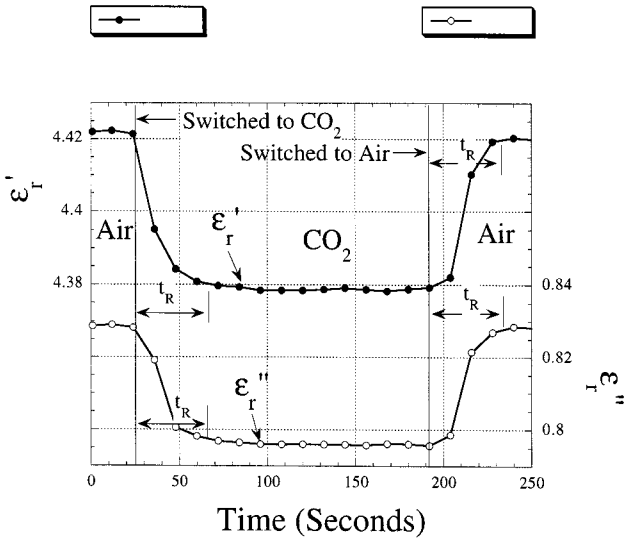

Fig. 10. Change in ε_r' and ε_r'' when the gas is switched from air to CO_2, and then back to air. The response time t_R, can be determined from the figure as less than 45 s.

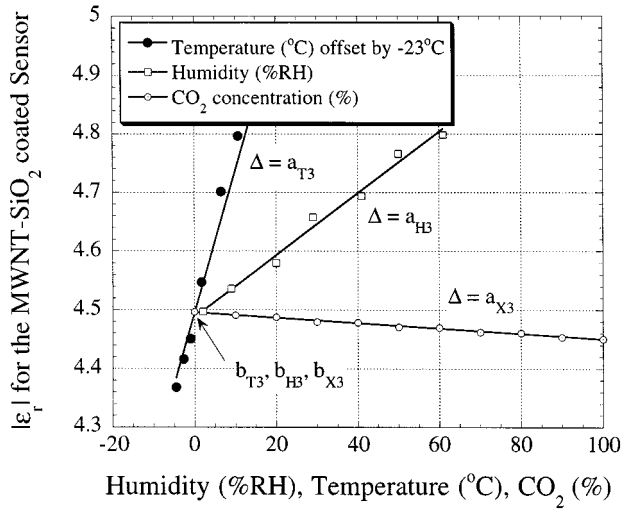

Fig. 11. Permittivity magnitude of the MWNT-based CO_2 sensor shifts linearly with CO_2, humidity, and temperature.

the response times are, respectively, 22, 16 and 14 min. The response times of switching from 100% to 0% humidity levels at 23 °C, 31 °C, and 42 °C are, respectively, 58, 36, and 34 min. Following a similar technique, the room temperature response time for O_2 was 4 min, and NH_3 about 2 min.

E. Humidity and Temperature Dependencies

Similar to many gas sensors, the carbon nanotube-based gas sensor also responds to temperature and humidity. As an illustration, Fig. 11 displays the effect of changing humidity, temperature, and CO_2 concentration on the complex permittivity magnitude of the MWNT-SiO_2 sensor coating. The effect of humidity and temperature can be eliminated by independently measuring humidity and temperature and performing a humidity-temperature calibration. Here, we illustrate the elimination of temperature and humidity effects on a CO_2 sensor by using three sensor elements, each of which responds to temperature and humidity in a unique way.

The three-element sensor array is comprised of a SiO_2-coated sensor, an uncoated sensor, and a MWNT-SiO_2 coated sensor. The SiO_2-coated and the plain sensors do not respond to CO_2, but both linearly respond in separable ways to humidity and temperature over the range investigated 0–60% RH and 18 °C–43 °C. Since their responses to both humidity and temperature are linear, the complex permittivity magnitude of the plain sensor ε_{r1}, and the SiO_2-coated sensor ε_{r2}, can be related to humidity and temperature as

$$\varepsilon_{r1} = (a_{T1}T + b_{T1}/2) + (a_{H1}H + b_{H1}/2) \quad (4)$$

$$\varepsilon_{r2} = (a_{T2}T + b_{T2}/2) + (a_{H2}H + b_{H2}/2). \quad (5)$$

H is humidity in %RH, T is temperature in °C, while a and b are coefficients experimentally determined by curve-fitting the changes in $|\varepsilon_r|$ as a function of temperature and humidity, and they are listed in Table I. In our experiment, T was offset by -23 °C (i.e., $T = 0$ means $T = 23$ °C in the real world); the offset is required since the sensor is initially calibrated at room temperature (23°C).

The humidity and temperature can then be determined by simultaneously solving (4) and (5)

$$\begin{bmatrix} T \\ H \end{bmatrix} = \frac{1}{a_{T1}b_{H2} - a_{T2}b_{H1}} \begin{bmatrix} b_{H2} & -b_{H1} \\ -a_{T2} & a_{T1} \end{bmatrix} - \begin{bmatrix} \varepsilon_{r1} - (b_{T1} + b_{H1})/2 \\ \varepsilon_{r2} - (b_{T2} + b_{H2})/2 \end{bmatrix}. \quad (6)$$

In practice, the coefficients a and b are only determined once after the fabrication of the sensor. The temperature and humidity are calculated by substituting the measured ε_{r1} and ε_{r2} into (6). For the MWNT-SiO_2 coated sensor the magnitude of the complex permittivity ε_{r3} can be related to humidity, temperature, and CO_2 with the equation:

$$\varepsilon_{r3} = (a_{T3}T + b_{T3}/3) + (a_{H3}H + b_{H3}/3) + (a_{X3}X + b_{X3}/3). \quad (7)$$

X is the percent volume of CO_2 present, T and H are the temperature and humidity values calculated with (6), and $a_{T3}, a_{H3}, a_{X3}, b_{T3}, b_{H3}$, and b_{X3} are coefficients determined by fitting the curves in Fig. 11 and are listed in Table I. Rearranging (7), the CO_2 concentration can be found as

$$X = \frac{\varepsilon_{r3} - a_{T3}T - a_{H3}H - (b_{T3} + b_{H3} + b_{X3})/3}{a_{X3}}. \quad (8)$$

Fig. 12(a) is an illustrative real-time measurement showing how the permittivity magnitude of the CO_2 sensor changes, at CO_2 concentration $= 0\%$ and 25%, in response to various humidity and temperature conditions. Due to the strong attraction of the MWNTs for water moisture, the response time of the CO_2 sensor suffers a dramatic increase in high humidity environments. Fig. 12(b) shows application of the sensor array to measurement of 0% and 25% CO_2 atmospheres in a variable temperature and humidity environment; the CO_2 percentage is calculated using (8) with data from Fig. 12(a). After a calibration, the calculated CO_2 levels in a given humidity and temperature environment are within an error margin of ± 3 CO_2%. Since the transitional periods over which the sensor reports spurious measurement values are clearly discernable, both due to the rapid rate of change and clearly incorrect values (e.g., 120%

TABLE I
REGRESSION COEFFICIENTS OF PLAIN, SiO_2 COATED, AND MWNT-SiO_2 COATED SENSORS

Coefficients	Plain Sensor	SiO_2-coated Sensor	MWNT-coated Sensor
a_T	$a_{T1} = 0.00089523$	$a_{T2} = 0.00193071$	$a_{T3} = 0.024175$
b_T	$b_{T1} = 1.01062$	$b_{T2} = 1.34392$	$b_{T3} = 4.49524$
a_H	$a_{H1} = 0.00011883$	$a_{H2} = 0.00064168$	$a_{H3} = 0.0052665$
b_H	$b_{H1} = 1.01051$	$b_{H2} = 1.34359$	$b_{H3} = 4.49472$
a_X	0	0	$a_{X3} = -0.00045769$
b_X	0	0	$b_{X3} = 4.49562$

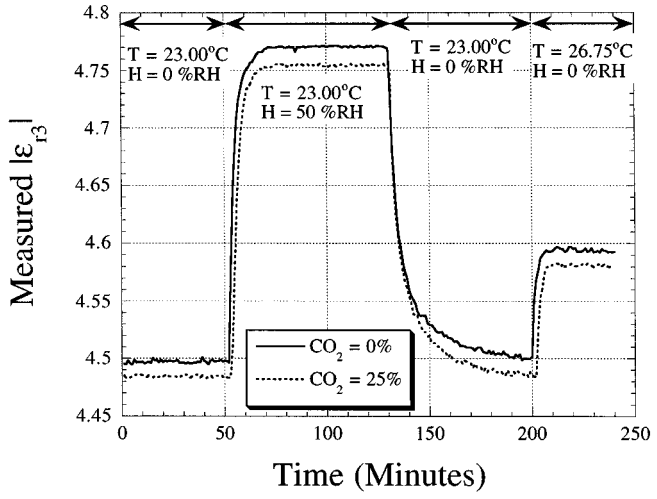

(a)

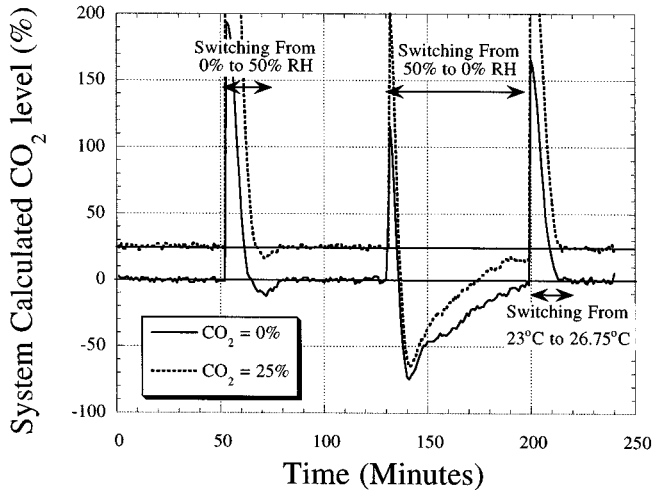

(b)

Fig. 12. (a) Permittivity magnitude of the MWNT-based CO_2 sensor, at zero and 25% CO_2 concentration, as it is exposed to different humidity and temperature conditions. (b) CO_2 concentration determined using measured data as corrected by (8) with calibration parameters of Table I; measurements are taken with CO_2 concentration kept at 0% and 25%. Outside of the transient region, upon reaching steady state measured results are within $\pm 3\%$. Since the different sensors have different response rates large errors occur when humidity and temperature change, an effect dominated by the slow desorption of moisture from the MWNTs.

CO_2), software routines could be readily implemented to keep the sensor tracking nominal steady-state values.

V. CONCLUSION

Application of multiwall carbon nanotubes (MWNTs) to O_2, CO_2, and NH_3 sensing has been reported. The sensor response is reversible for O_2 and CO_2, but irreversible for NH_3. Sensor response time is approximately 45 s, 4 min, and 2 min for CO_2, O_2, and NH_3, respectively. The MWNTs are used in combination with a passive, remote query sensor platform, so no direct wire connections or internal batteries are needed to power the sensor. These operational characteristics make the gas sensor attractive for long-term wireless monitoring applications, such as monitoring of environmental NH_3 levels in an industrial area, or measuring the CO_2 levels in food or medicine packages to check for product spoilage.

It is found that ε_r'' (proportional to conductivity) of the MWNTs shifts lower when the sensor is exposed to either CO_2 or NH_3 since both gases are reducing agents that inject electrons to the p-type MWNTs [28] reducing the number of holes and hence conductivity. Conversely, ε_r'' of the MWNTs is higher when the sensor is exposed to O_2 since O_2, being an oxidizing agent, attracts electrons from the *p*-type MWNTs and increases the number of conducting holes. Our observations on ε_r'' (conductivity) decreasing with CO_2 adsorption are consistent with those reported elsewhere [31], [32]. Absorption of CO_2 and O_2 also lowers ε_r' of the MWNTs because more CO_2 and O_2 molecules are absorbed into MWNTs compared to N_2, which reduce the average ε_r' of the MWNT layer since the ε_r' of CO_2 and O_2 are much lower than MWNTs. The sensor shows both reversible and irreversible changes when detecting NH_3 due to the weak physisorption of NH_3 that causes the reversible change and the strong chemisorption of NH_3 that causes the irreversible change.

To eliminate the deleterious effects of humidity and temperature on the MWNT-based CO_2 sensor, measured values are calibrated against the response of both a SiO_2-coated sensor, and a plain (uncoated) sensor, neither of which respond to CO_2, and both uniquely respond to temperature and humidity. Using the described calibration algorithm of (8) enables CO_2 concentrations to be measured to within ± 3 CO_2% in a changing

humidity and temperature environment. For operation within 0–60% RH and 18 °C–43 °C the sensors respond linearly to humidity and temperature, therefore a straight-forward linear calibration routine can be used with success. At higher temperatures and humidity levels the sensor responses are nonlinear, so a higher-order calibration routine would be needed to maintain sensor accuracy.

REFERENCES

[1] W. A. de Heer, A. Chatelain, and D. Ugarte, "A carbon nanotube field-emission electron source," *Science*, vol. 270, pp. 1179–1180, 1995.

[2] S. Tans, A. Verschueren, and C. Dekker, "Room-temperature transistor based on a single carbon nanotube," *Nature*, vol. 393, pp. 49–52, 1998.

[3] R. Martel, T. Schmidt, H. R. Shea, T. Hertel, and Ph. Avouris, "Single- and multiwall carbon nanotubes field-effect transistor," *Appl. Phys. Lett.*, vol. 73, pp. 2447–2449, 1998.

[4] S. Tan, M. Devoret, H. Dai, A. Thess, R. Smalley, L. Geerligs, and C. Dekker, "Individual single-wall carbon nanotubes as quantum wires," *Nature*, vol. 386, pp. 474–477, 1997.

[5] Z. Yao, H. Postma, L. Balents, and C. Dekker, "Carbon nanotube intramolecular junctions," *Nature*, vol. 402, pp. 273–276, 1999.

[6] R. H. Baughman, C. Cui, A. A. Zakhidov, Z. Iqbal, J. N. Barasci, G. M. Spinks, G. G. Wallace, A. Mazzoldi, D. de Rossi, A. G. Rinzler, O. Jaschinski, S. Roth, and M. Kertesz, "Carbon nanotube actuators," *Science*, vol. 284, pp. 1340–1342, 1999.

[7] T. Rueckes, K. Kim, E. Joselevich, G. Y. Tseng, C. Cheung, and C. M. Lieber, "Carbon nanotube-based nonvolatile random access memory for molecular computing," *Science*, vol. 289, pp. 94–97, 2000.

[8] J. Kong, N. R. Franklin, C. Zhou, M. G. Chapline, S. Peng, K. Cho, and H. Dai, "Nanotube molecular wires as chemical sensors," *Science*, vol. 287, pp. 622–625, 2000.

[9] M. Bienfait, B. Asmussen, M. Johnson, and P. Zeppenfeld, "Methane mobility in carbon nanotubes," *Surf. Sci.*, vol. 460, pp. 243–248, 2000.

[10] E. Ivers-Tiffee, K. H. Hardtl, W. Menesklou, and J. Riegel, "Principles of solid state oxygen sensors for lean combustion gas control," *Electrochim. Acta*, vol. 47, pp. 807–814, 2001.

[11] J. W. Erisman, R. Otjes, A. Hensen, P. Jongejan, P. van den Bulk, A. Khlystov, H. Mols, and S. Slanina, "Instrument development and application in studies and monitoring of ambient ammonia," *Atmos. Environ.*, vol. 35, pp. 1913–1922, 2001.

[12] S. L. Well and J. DeSimone, "CO_2 technology platform: An important tool for environmental problem solving," *Angew. Chem. Int. Ed.*, vol. 40, pp. 518–527, 2001.

[13] T. Lindgren, D. Norback, K. Anderson, and B. Dammstrom, "Cabin environment and perception of cabin air quality among commercial aircrew," *Aviation, Space, Environ. Med.*, vol. 71, no. 8, pp. 774–482, 2000.

[14] N. Sheppard, R. Tucker, and S. Salehi-Had, "Design of a conductimetric pH microsensor based on reversibly swelling hydrogels," *Sens. Actuators B*, vol. 10, pp. 73–77, 1993.

[15] P. Dalgaard, O. Mejlholm, and H. H. Huss, "Application of an interactive approach for development of a microbial model predicting the shelf-life of packed fish," *Int. J. Food Microbiol.*, vol. 38, pp. 169–179, 1997.

[16] H.-E. Endres, R. Hartinger, M. Schwaiger, G. Gmelch, and M. Roth, "A capacitive CO_2 sensor system with suppression of the humidity interference," *Sens. Actuators B*, vol. 57, pp. 83–87, 1999.

[17] M. S. Lee and J. U. Meyer, "A new process for fabricating CO_2-sensoing layers based on $BaTiO_3$ and additives," *Sens. Actuators B*, vol. 68, pp. 293–299, 2000.

[18] S. Matsubara, S. Kaneko, S. Morimoto, S. Shimizu, T. Ishihara, and Y. Takita, "A practical capacitive type CO_2 sensor using CeO_2/$BaCO_3$/CuO ceramics," *Sens. Actuators B*, vol. 65, pp. 128–132, 2000.

[19] J. F. Currie, A. Essalik, and J. C. Marusic, "Micromachined thin film solid state electrochemical CO_2, NO_2, and SO_2 gas sensors," *Sens. Actuators B*, vol. 59, pp. 235–241, 1999.

[20] K. G. Ong and C. A. Grimes, "A resonant printed-circuit sensor for remote query monitoring of environmental parameters," *Smart Mater. Struct.*, vol. 9, pp. 421–428, 2000.

[21] K. G. Ong, C. A. Grimes, C. L. Robbins, and R. S. Singh, "An inductor-capacitor resonant circuit remote query sensor: Design and application," *Sens. Actuators A*, vol. 95, pp. 33–43, 2001.

[22] Chemat Technology, Inc., Northridge, CA.

[23] S. Ramo, J. R. Whinnery, and T. Van Duzer, *Fields and Waves in Communication Electronics*. New York: Wiley, 1984, ch. 13.

[24] H. E. Brian, "Printed inductors and capacitors," *Tele-Tech Electron. Ind.*, vol. 14, pp. 68–69, 1954.

[25] G. H. Markx and C. L. Davey, "The dielectric properties of biological cells at radiodfrequencies: Applications in biotechnology," *Enzyme Microbial Technol.*, vol. 25, pp. 161–171, 1999.

[26] H. E. Endres and S. Drost, "Optimization of the geometry of gas-sensitive interdigital capacitor," *Sens. Actuators B*, vol. 4, pp. 95–98, 1991.

[27] R. Andrews, D. Jacques, A. M. Rao, F. Derbyshire, Q. Qian, F. Fan, E. C. Dickey, and J. Chen, "Continuous production of aligned carbon nanotubes: A step closer to commersial realization," *Chem. Phys. Lett.*, vol. 303, pp. 467–474, 1999.

[28] O. K. Varghese, P. D. Kichambare, D. Gong, K. G. Ong, E. C. Dickey, and C. A. Grimes, "Gas sensing characteristics of multiwall carbon nanotubes," *Sens. Actuators B*, vol. 81, pp. 32–41.

[29] P. L. Walker Jr., *Chemistry and Physics of Carbon*. New York: Marcel Dekker, 1970, vol. 6.

[30] G. U. Sumanasekera, C. K. W. Adu, S. Fang, and P. C. Eklund, "Effects of gas adsorption and collisions on electrical transport in single walled carbon nanotubes," *Phy. Rev. Lett.*, vol. 85, pp. 1096–1099, 2000.

[31] C. Marliere, P. Poncharal, L. Vaccarini, and A. Zahab, "Effect of gas adsorption on the electrical properties of single-walled carbon nanotubes mats," in *Mat. Res. Soc. Symp. Proc.*, vol. 539, 2000, pp. 173–178.

[32] I. Stepanek, L. C. de Menorval, R. Edwards, and P. Bernier, "Carbon nanotubes and gas adsorption," in *AIP Conf. Proc.*, vol. 486, 1999, pp. 456–461.

Keat Ghee Ong received the B.S., M.S., and Ph.D. degrees in electrical engineering from the University of Kentucky, Lexington, in 1997, 1998, and 2000, respectively.

He is currently a research associate with the Pennsylvania State University, University Park. Ong's areas of expertise include magnetism, rf and acoustic-based sensors, nanoporous metal oxides and carbon nanotubes, efficient multi-element electrically small antennas, and measurement technique and instrument automation. He is on the editorial board of two sensor-related journals, and is the co-author of one book chapter and over 30 publications in archival journals and conference proceedings.

Kefeng Zeng received the B.S. degree from the Department of Electronics and Information Engineering, Huazhong University of Science and Technology, Wuhan, China, in 1995.

From 1995 to 1999, he worked at the First Research Institute of the Ministry of Public Security, Beijing, China. He finished the M.S. program at the National University of Singapore in 2001. Currently, he is a Ph.D. student at the Electrical Engineering Department, Pennsylvania State University, University Park.

Craig A. Grimes (M'87) received the B.S. degrees in electrical engineering and physics from the Pennsylvania State University (PSU), University Park, in 1984, and the M.S. and Ph.D. degrees in electrical engineering from the University of Texas, Austin, in 1986 and 1990, respectively.

From 1994 to 2001, he was a member of the Electrical and Computer Engineering Department, University of Kentucky, Lexington, where he was the Frank J. Derbyshire Professor. He is currently an Associate Professor with PSU and member of the Materials Research Institute. His research interests include remote query chemical and environmental sensors, nano-dimensional metal-oxide thin film architectures, propagation and control of electromagnetic energy, and carbon nanotube-based electronic devices. He has contributed to over 100 archival journal publications, six book chapters, and is co-author of the book *The Electromagnetic Origin of Quantum Theory and Light* published by World Scientific.